Coherence Maps for Wind-Forced Quasigeostrophic Flows*

PETER MÜLLER

Department of Oceanography, University of Hawaii at Manoa, Honolulu, Hawaii

(Manuscript received 11 November 1996, in final form 24 February 1997)

ABSTRACT

Coherence maps are a useful tool to study the oceanic response to atmospheric forcing. For a specific frequency band these maps display the coherence between the oceanic current (or pressure) at a single mooring location and the atmospheric forcing field at other locations as a function of separation. This paper calculates such coherence maps from a simple linear quasigeostrophic model forced by a statistically stationary and homogeneous wind field. The calculated coherence maps show values less than one. Such values are not due to the presence of noise but are a consequence of the ocean being forced at many locations. The maps also show characteristic patterns with maxima either at the mooring location or away from it. The locations of the maxima do not indicate the locations of the forcing but instead reflect the scales of the atmospheric forcing spectrum and of the Green's function of the potential vorticity equation. Coherence maps can be used to estimate the Green's function in a multiple regression analysis. The presence of noise or nonlinearities in the system can be inferred from the multiple coherence, which is a number. Emphasis is on understanding the information content of coherence maps, not on reproducing observed maps. The results can be generalized to other systems where response and forcing are related by a Green's function.

1. Introduction

In studying the oceanic response to wind forcing, Brink (1989) introduced an important new analytical tool: the cross-covariance or coherence map, which displays the cross-covariance or coherence between the oceanic current (or pressure) at a fixed point (the mooring location) and the wind stress curl field at other locations as a function of separation in a specific frequency band. For various subinertial frequencies such coherence maps have been estimated by Brink (1989) and Samelson (1990) using current observations in the western and eastern North Atlantic and wind fields from the Fleet Numerical Oceanographic Center (FNOC) and by Luther et al. (1990) and Chave et al. (1992) using barotropic current and pressure observations in BEMPEX (Barotropic Electromagnetic and Pressure Experiment) and FNOC winds. These maps show significant nonzero coherences, often with maxima away from the mooring location. These are highly significant observations since they provide the first direct evidence that part of the subinertial variability in the ocean is directly forced by the atmospheric wind stress, a notion that has earlier been asserted by Frankignoul and Müller (1979), Willebrand et al. (1980), and others by more indirect means. The maxima in the coherence maps, at the mooring location or away from it, have often been interpreted as the location of the forcing.

The observations immediately prompted theoretical investigations to rationalize the findings. Brink (1989), Samelson (1990), and later Lippert and Müller (1995) all calculated coherence maps from a simple linear quasigeostrophic model with stochastic wind forcing, for comparison with the observed maps. The model has a flat bottom and no mean currents. The forcing is assumed to be statistically homogeneous and described either by its autocovariance function in separation space or by its spectrum in wavenumber space. Choosing certain idealized but reasonable spectra or autocovariance functions, all authors were able to reproduce basic aspects of the observed coherence maps, including nonlocal maxima away from the mooring location. Samelson (1989) and Samelson and Shrayer (1991) used inhomogeneous forcing and a more complex basic state to explain aspects of the coherence maps that were not reproduced by the simple model.

In this paper we analyze theoretically the information contained in cross-covariance or coherence maps, using the simple quasigeostrophic forcing model as an example. We specifically show that for this model the location of the maxima reflects the scales of the forcing spectrum and the scales of the Green's function of the quasigeostrophic potential vorticity equation. In models with statistically homogeneous forcing, the location of the maxima does not indicate the location of the forcing.

*School of Ocean and Earth Science and Technology Contribution Number 4499.

Corresponding author address: Dr. Peter Müller, Department of Oceanography, University of Hawaii at Manoa, 1000 Pope Road, Honolulu, HI 96822.
E-mail: pmuller@iniki.soest.hawaii.edu

This point can be made quite generally but it is most easily made in a horizontally unbounded ocean where the response to statistically homogeneous forcing is also statistically homogeneous. Brink (1989) and Samelson (1990) consider the response in a meridional channel. This complicates the algebra because the response becomes inhomogeneous, despite homogeneous forcing, and because an additional length scale, the basin width, enters the calculation.

We first discuss the simple quasigeostrophic model and its Green's function. The Green's function describes how the forcing at different locations contributes to the response at a specific point. These different contributions can interfere, either constructively or destructively. This interference determines which forcing locations contribute to the signal at a specific point. As an example, we calculate the response to a single ''wave.'' Next we consider statistically homogeneous and stationary forcing. We follow observational practice and perform our analyses in frequency space. Thus, all statistical quantities in this paper are spectra in frequency space. In regards to space, the analysis would be simplest in wavenumber space. The Fourier amplitudes at different wavenumbers are uncorrelated for statistically homogeneous fields. The potential vorticity equation linearly relates the Fourier amplitudes of the response to those of the forcing. However, the spatial Fourier amplitudes of the response cannot be estimated from measurements at a single mooring location, only from space-resolving measurements such as altimetric measurements. Therefore, observationalists who only have data from one or a few moorings must carry out their analysis in separation space. They can only estimate cross-covariance or coherence maps, that is, the cross-covariance or coherence between the response at the mooring location and the forcing at other locations as a function of separation. We calculate these maps from the simple forcing model and analyze both generally and by example how the basic features of these maps depend on the scales of the forcing and the Green's function. The emphasis is not on reproducing observed maps but on understanding their information content. We then suggest that cross-covariance maps be used to estimate the Green's function. The noise can then be estimated from the multiple coherence, which is a number.

2. Potential vorticity equation

The linear quasigeostrophic response of a homogeneous, beta-plane, constant depth ocean to wind stress forcing is given by the potential vorticity equation

$$(\partial_t + \nu)(\partial_x\partial_x + \partial_y\partial_y - R_0^{-2})p(x, y, t) + \beta_0\partial_x p(x, y, t) = F(x, y, t), \tag{2.1}$$

where p is the pressure, t time, x the zonal coordinate, y the meridional coordinate, β_0 the meridional gradient of the Coriolis parameter, R_o the external Rossby radius of deformation, F the forcing, and ν a Rayleigh friction coefficient. Friction is included to limit the response in a horizontally unbounded ocean. In most cases we assume friction to be small and only use it as a tool to properly deal with the singularities of the frictionless theory. In these cases the friction coefficient is set to zero in the final result.

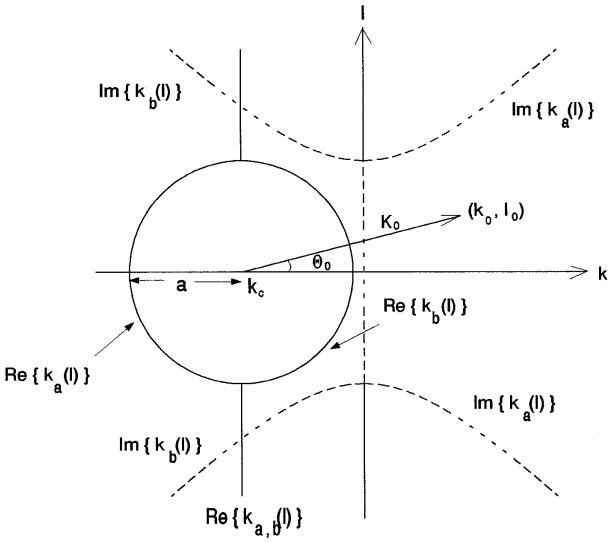

FIG. 1. Wavenumber plane displaying (i) the dispersion circle with center at $(k, l) = (k_c, 0)$ and radius a, (ii) the real and imaginary parts of the functions $k_a(l)$ and $k_b(l)$, and (iii) the ''polar coordinates'' K_0 and θ_0.

Without forcing and friction the potential vorticity equation has free wave solutions of the form $p(x, y, t) \sim \exp[i(kx + ly - \omega t)]$, called Rossby waves, with dispersion relation

$$\omega = \Omega(k, l) = -\frac{\beta_0 k}{k^2 + l^2 + R_0^{-2}}. \tag{2.2}$$

Here k and l are the zonal and meridional wavenumber component and ω is the frequency. In the wavenumber plane the locus $\Omega(k, l) = \omega = \text{const}$ represents a circle with center at $(k, l) = (k_c, 0)$, where

$$k_c(\omega) = -\frac{\beta_0}{2\omega} \tag{2.3}$$

and radius

$$a(\omega) = (k_c^2 - R_o^{-2})^{1/2} \tag{2.4}$$

(see Fig. 1). The group velocity points toward the center of the circle. Such free waves only exist for $|\omega| < \omega_{\max} = \beta_0 R_o/2$.

In frequency space the potential vorticity equation takes the form

$$(\partial_x\partial_x + \partial_y\partial_y - R_o^{-2})p(x, y, \omega) - 2i\tilde{k}_c\partial_x p(x, y, \omega) = \frac{i}{\tilde{\omega}}F(x, y, \omega), \tag{2.5}$$

where $\tilde{\omega} = \omega + i\nu$ and the tilde on k_c indicates that ω is replaced by $\tilde{\omega}$ in the definition (2.3). Upon substitution of $\hat{p} = p \exp(-i\tilde{k}_c x)$ this equation transforms to the inhomogeneous Helmholtz equation

$$(\partial_x\partial_x + \partial_y\partial_y + \tilde{a}^2)\hat{p}(x, y, \omega) = \frac{i}{\tilde{\omega}}F(x, y, \omega)e^{-i\tilde{k}_c x}, \quad (2.6)$$

where the tilde on a again indicates that ω is replaced by $\tilde{\omega}$ in the defintion (2.4). The Helmholtz equation has been studied extensively (e.g., Morse and Feshbach 1953), especially its Green's functions.

3. Green's function

The solution of the potential vorticity equation (2.1) can be written as a convolution integral

$$p(x, y, \omega) = \int dx' \int dy' G(x - x', y - y', \omega)F(x', y', \omega) \quad (3.1)$$

with the Green's function

$$G(x, y, \omega) = \frac{1}{4\tilde{\omega}}H_0^{(2)}(\tilde{a}_- R)e^{i\tilde{k}_c x} \quad (3.2)$$

where $H_0^{(2)}$ is a Hankel function of the second kind of zeroth order, $R = (x^2 + y^2)^{1/2}$, and $\tilde{a}_-$ is the root with the negative imaginary part. This particular root and Hankel function are chosen so that the Green's function decays asymptotically. For $|\omega| < \omega_{\max}$, this requires the inclusion of friction. The response to a point source $F(x, y, \omega) = \delta(x - x_0)\delta(y - y_0)$ is $p(x, y, \omega) = G(x - x_0, y - y_0, \omega)$. In the following we drop the parametric dependence on ω.

For a meridional channel, as used for example by Brink (1989), we can Fourier transform to meridional wavenumber space and obtain

$$p(x, l) = 2\pi \int dx' G(x - x', l)F(x', l) \quad (3.3)$$

with Green's function

$$G(x, l) = -\frac{1}{2\pi}\frac{1}{2\tilde{\omega}\tilde{m}_-}\begin{cases} e^{i\tilde{k}_a x} & \text{for } x > 0 \\ e^{i\tilde{k}_b x} & \text{for } x < 0, \end{cases} \quad (3.4)$$

where

$$\tilde{k}_a(l) = \tilde{k}_c - \tilde{m}_- \quad (3.5a)$$

$$\tilde{k}_b(l) = \tilde{k}_c + \tilde{m}_- \quad (3.5b)$$

and

$$\tilde{m}^2(l) = \tilde{a}^2 - l^2. \quad (3.6)$$

The minus subscript again indicates that the root with the negative imaginary part is chosen. This choice again assures that the Green's function decays asymptotically in both directions. The functions $k_{a,b}(l)$ are also shown in Fig. 1 for a case where $|\omega| < \omega_{\max}$. For $|l| \le a$ the wavenumbers $k_{a,b}(l)$ lie on the dispersion circle and are thus resonance wavenumbers that satisfy the dispersion relation.

In an unbounded ocean Fourier transformation in both coordinates leads to

$$p(k, l) = (2\pi)^2 G(k, l)F(k, l) \quad (3.7)$$

with Green's function

$$G(k, l) = \frac{1}{(2\pi)^2}\frac{-i}{(k^2 + l^2 + R_0^{-2})(\tilde{\omega} - \Omega(k, l))}. \quad (3.8)$$

The Green's function $G(k, l)$ shows the typical resonance behavior $(\tilde{\omega} - \Omega(k, l))^{-1}$. It would lead to singularities on the dispersion circle if friction were not included. Equation (3.7) is the most compact form of the solution for an infinite ocean. The Fourier coefficients of the response and forcing are simply proportional with the factor of proportionality given by the Green's function.

The Fourier components $p(x, l)$ and $p(k, l)$ cannot be inferred from single point ocean measurements. The solutions (3.3) and (3.7) can therefore not be tested directly. However, these solutions lead to different representations of the solution in physical space; namely,

$$p(x, y) = 2\pi \int dx' \int dl G(x - x', l)F(x', l)e^{ily} \quad (3.9)$$

and

$$p(x, y) = (2\pi)^2 \int dk \int dl G(k, l)F(k, l)e^{i(kx+ly)}. \quad (3.10)$$

The different representations (3.1), (3.9), and (3.10) show how the forcing at different locations or wavenumbers contribute to the response at position (x, y). The different contributions interfere either constructively or destructively.

4. Response to single wave

The Green's function describes the response to a point source. Here we calculate the response to a distributed source in order to understand which forcing locations contribute to the response at a single point. Specifically, we calculate the response to a single Fourier component $F(x, y) = \exp[i(k_0 x + l_0 y)]$ or $F(k, l) = \delta(k - k_0)\delta(l - l_0)$. The representation (3.10) immediately gives the response

$$p(x, y) = (2\pi)^2 G(k_0, l_0)e^{i(k_0 x + l_0 y)}. \quad (4.1)$$

However, if we want to know how different locations contribute to this response at (x, y), we have to use representation (3.1), which yields

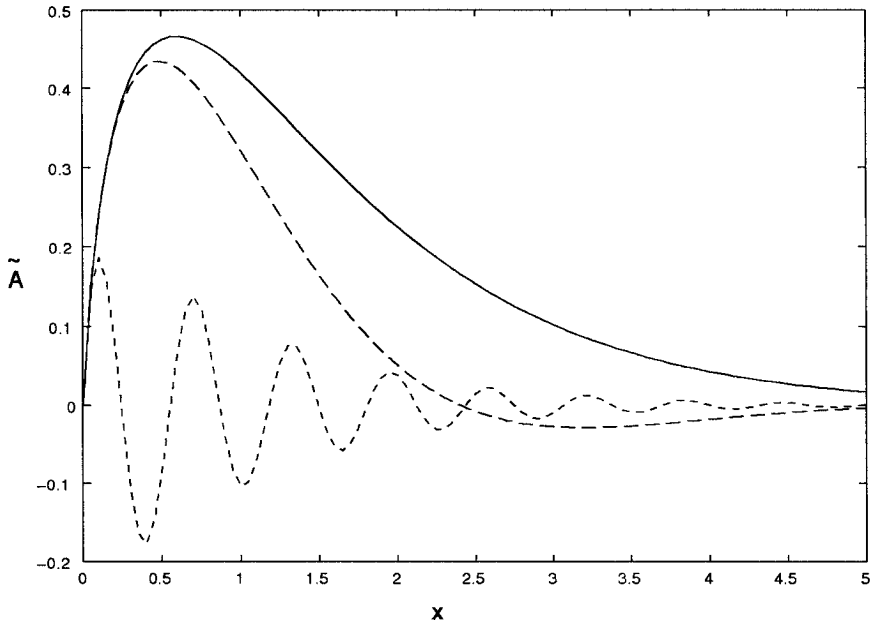

FIG. 2. Contributions from different radii for frequencies larger than the maximal Rossby wave frequency. The figure shows the function $\tilde{A}(x) = xK_0(x)J_0(K_0x/b)$ for $K_0/b = 0.1$ (solid), $K_0/b = 1$ (long dash), and $K_0/b = 10$ (short dash).

$$p(x, y) = e^{i(k_0x+l_0y)} \int dx' \int dy' G(-x', -y') e^{i(k_0x'+l_0y')}. \quad (4.2)$$

In the limit $\nu \to 0$ we find

$$p(x = 0, y = 0) = \int_0^\infty dRR \int_0^{2\pi} d\varphi \frac{1}{4\omega} H_0^{(2)}(\tilde{a}_- R) e^{iK_0R\cos(\varphi-\theta_0)}, \quad (4.3)$$

where $(k_0 - k_c) = K_0\cos\theta_0$ and $l_0 = K_0\sin\theta_0$. Thus, K_0 and θ_0 are the magnitude and direction of the wavenumber vector (k_0, l_0) in a frame shifted by k_c (see Fig. 1). The contributions from different radii are given by

$$A(R) = \frac{1}{4\omega} RH_0^{(2)}(\tilde{a}_- R) \int_0^{2\pi} d\varphi e^{iK_0R\cos(\varphi-\theta_0)} \quad (4.4a)$$

$$= \frac{1}{4\omega} RH_0^{(2)}(\tilde{a}_- R) 2\pi J_0(K_0R), \quad (4.4b)$$

where J_0 is a Bessel function of the first kind of zeroth order. For $|\omega| > \omega_{\max}$ we have $\tilde{a}_- \to -ib$ for $\nu \to 0$ where $b = (R_o^{-2} - k_c^2)^{1/2}$, and we find

$$A(R) = \frac{i}{\omega} R\tilde{K}_0(bR) J_0(K_0R), \quad (4.5)$$

where $\tilde{K}_0$ is the modified Bessel function of the second kind of zeroth order and where we made use of the identity

$$H_0^{(2)}(-ix) = \frac{2i}{\pi} \tilde{K}_0(x).$$

The tilde has been added to the standard symbol for the modified Bessel function in order to distinguish it from the magnitude K_0 of the wavenumber vector. The modified Bessel function $\tilde{K}_0(x)$ decreases exponentially to zero. The function

$$\tilde{A}(R) = x\tilde{K}_0(x) J_0\left(\frac{K_0}{b}x\right)$$

is displayed in Fig. 2 for three different values of K_0/b. The figure shows that the major contributions at a point (x, y) come from within a circle of radius $O(2b)$.

For $|\omega| < \omega_{\max}$ we have $\tilde{a}_- \to a$ for $\nu \to 0$, where a is the radius of the dispersion circle. In this case the function $A(R)$ does not decay to zero for $R \to \infty$ but has the asymptotic behavior

$$A(R) \sim \frac{1}{\omega} \frac{1}{\sqrt{K_0a}} [e^{i(K_0-a)R} + ie^{-i(K_0+a)R}]. \quad (4.6)$$

The contributions to the response at a point (x, y) thus come from all values of R. Since $A(R)$ is an oscillating function, most of the contributions interfere destructively and cancel, unless $K_0 = a$, that is, unless the ocean is forced in resonance. In this case

$$A(R) \sim 1 + i \exp(-2iK_0R) \quad (4.7)$$

and $A(R)$ contains a constant contribution.

The contributions from different directions are given by

$$B(\varphi) = \int_0^\infty dRR \frac{1}{4\omega} H_0^{(2)}(\tilde{a}_- R) e^{iK_0R\cos(\varphi-\theta_0)}. \quad (4.8)$$

Upon substitution of the integral representation

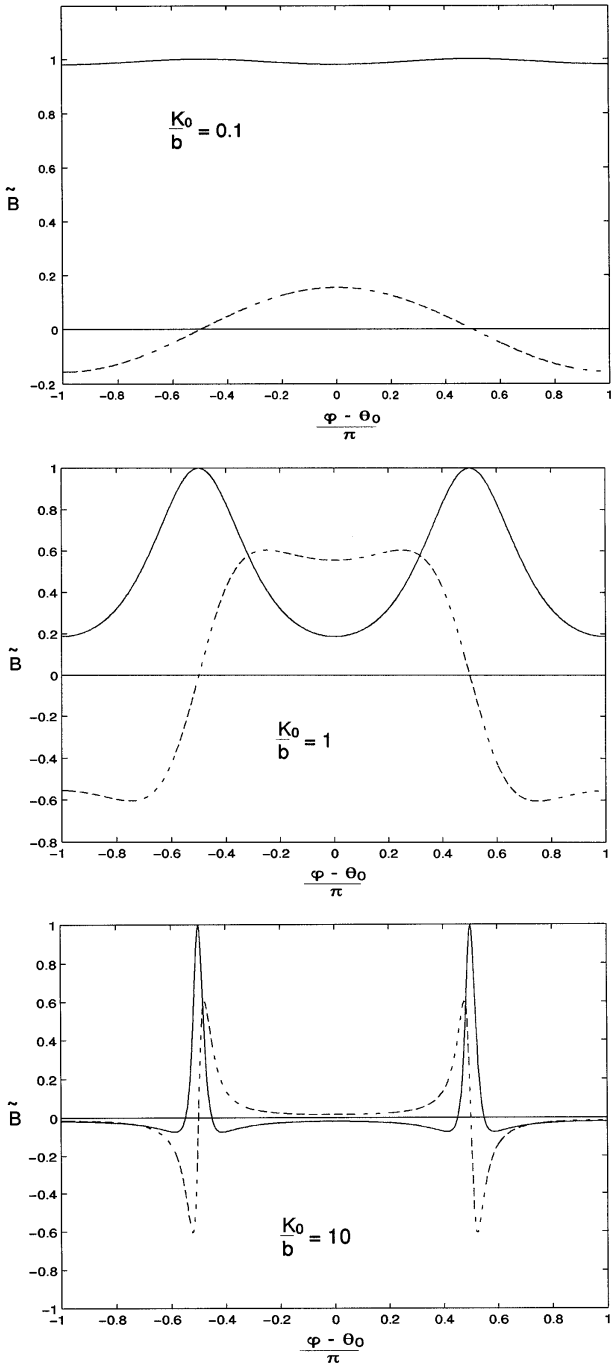

FIG. 3. Contributions from different angles for frequencies larger than the maximal Rossby wave frequency. The figure shows the real part (solid) and imaginary part (dash) of $\tilde{B}$ as a function of $\phi - \theta_0$ for three different values of K_0/b.

$$H_0^{(2)}(x) = \frac{2i}{\pi}\int_0^\infty du e^{-ix\cosh u}, \tag{4.9}$$

one can carry out the integration over R and obtain

$$B(\varphi) = -\frac{1}{4\omega}\frac{2i}{\pi}\frac{1}{\tilde{a}_-^2}\int_0^\infty du \frac{1}{(\tilde{p} - \cosh u)^2}, \tag{4.10}$$

where

$$\tilde{p} = \frac{K_0}{\tilde{a}_-}\cos(\varphi - \theta_0).$$

The integration over u gives

$$\tilde{B}(\varphi) = \int_0^\infty \frac{1}{(\tilde{p} - \cosh u)^2}$$

$$= \frac{1}{1 - \tilde{p}^2}\left(1 - \frac{\tilde{p}}{\sqrt{\tilde{p}^2 - 1}} \times \ln\frac{1 - \tilde{p} - \sqrt{\tilde{p}^2 - 1}}{1 - \tilde{p} + \sqrt{\tilde{p}^2 + 1}}\right). \tag{4.11}$$

Figure 3 shows the function $\tilde{B}(\varphi)$ in the limit $\tilde{a}_- \to -ib$ for three different values of K_0/b. For $K_0/b \to 0$ we find Re $[\tilde{B}(\varphi)] \to 1$ and Im$[\tilde{B}(\varphi)] \to 0$. An observer will thus see ''light'' coming in from all directions. As K_0/b becomes larger the response becomes more and more concentrated at the points $(\varphi - \theta_0) = \pm\pi/2$, that is, at the points where $\tilde{p}$ vanishes. ''Light'' only comes in from directions perpendicular to θ_0. Figure 4 shows the analogous results for $\tilde{a}_- \to a$. For small K_0/b the distribution is again broad. For $K_0/a = 1$, that is, for forcing at a resonant wavenumber, the distribution is sharply centered at $(\varphi - \theta_0) = 0$ where it becomes infinite. Since the group velocity of Rossby waves points toward the center of the dispersion circle, the signal thus comes toward the observer from a direction opposite to that of the group velocity vector, consistent with physical expectations. For K_0/a larger than one, $\tilde{B}(\varphi)$ becomes concentrated at the two directions $(\varphi - \theta_0) = \pm\cos^{-1}(a/K_0)$ where $\tilde{p} = 1$. These are the directions toward the points where straight lines through (k_0, l_0) become tangent to the dispersion circle. Actually, $\tilde{B}(\varphi)$ is a generalized function or distribution in this case, arising from the fact that for

$$\varphi - \theta_0 \in \left[-\cos^{-1}\frac{a}{K_0}, \cos^{-1}\frac{a}{K_0}\right]$$

there is always a u value for which the integrand in (4.10) becomes singular in the limit $\tilde{a}_- \to a$. It is important for our argument later on that the functions $A(R)$ and $B(\varphi)$ do not change their form if the geostrophic velocity components $u = -\partial_y p$ and $v = \partial_x p$ are considered instead of the pressure p. The functions are only multiplied by a factor $-il_0$ or ik_0.

The above results can more explicitly be shown for the case $l_0 = 0$, that is, for forcing that is independent of the meridional coordinate. In this case we find from (3.9)

$$p(x, y) = -\frac{1}{2\tilde{\omega}\tilde{a}_-}\left[e^{i\tilde{k}_a x}\int_{-\infty}^{x} dx' e^{i(k_0-\tilde{k}_a)x'} + e^{i\tilde{k}_b x}\int_{x}^{\infty} dx' e^{i(k_0-\tilde{k}_b)x'}\right]. \quad (4.12)$$

The first term represents the contributions from the west, the second term the contributions from the east. For forcing at resonant wavenumber $k_0 = k_a$, which generates short Rossby waves with an eastward group velocity, the contributions from the west interfere constructively, whereas the contributions from the east interfere destructively and cancel to a large extent. For forcing at resonant wavenumber $k_0 = k_b$, which generates long Rossby waves with a westward group velocity, the situation is reversed.

5. Coherence maps

We now assume that the forcing function $F(x, y, t)$ is a random function; especially, we assume that it is a zero-mean, statistically stationary, and homogeneous process. Since we consider an unbounded ocean and include friction, the oceanic response $p(x, y, t)$ is also a zero-mean, statistically stationary, and homogeneous process (e.g., Müller 1996). For such processes the Fourier amplitudes $F(k, l, \omega)$ and $p(k, l, \omega)$ at different wavenumbers and frequencies are uncorrelated. The forcing and response will be described by their spectrum in frequency space and by their spectrum in wavenumber space or their autocovariance function in separation space. Spectrum and covariance function are related by a Fourier transformation. The cross-spectrum between response and forcing is defined by

$$S_{pF}(k, l, \omega)\delta(k - k')\delta(l - l')\delta(\omega - \omega') = \langle p^*(k, l, \omega)F(k', l', \omega')\rangle, \quad (5.1)$$

where angle brackets denote the ensemble average. The cross-spectrum is given for our simple model by

$$S_{pF}(k, l, \omega) = (2\pi)^2 G^*(k, l, \omega)S_{FF}(k, l, \omega) \quad (5.2)$$

as an immediate consequence of the direct proportionality between $p(k, l, \omega)$ and $F(k, l, \omega)$ [see (3.7)]. This direct proportionality implies that the coherence squared

$$\gamma^2_{pF}(k, l, \omega) = \frac{|S_{pF}(k, l, \omega)|^2}{S_{pp}(k, l, \omega)S_{FF}(k, l, \omega)} \quad (5.3)$$

is identical to one for our model. If observational estimates $\tilde{S}_{pF}(k, l, \omega)$, $\tilde{S}_{pp}(k, l, \omega)$, and $\tilde{S}_{FF}(k, l)$ were used, the coherence would generally be less than one and this would indicate the presence of noise (or nonlinearities or other forcing fields).

As discussed in the introduction, oceanographers working with data from a single mooring can only consider the cross-covariance function between the response at the mooring position (x, y) and the forcing at positions $(x + \Delta x, y + \Delta y)$, which is defined by

$$C_{pF}(\Delta x, \Delta y, \omega)\delta(\omega - \omega') = \langle p^*(x, y, \omega)F(x + \Delta x, y + \Delta y, \omega')\rangle \quad (5.4)$$

and is given for our simple model by

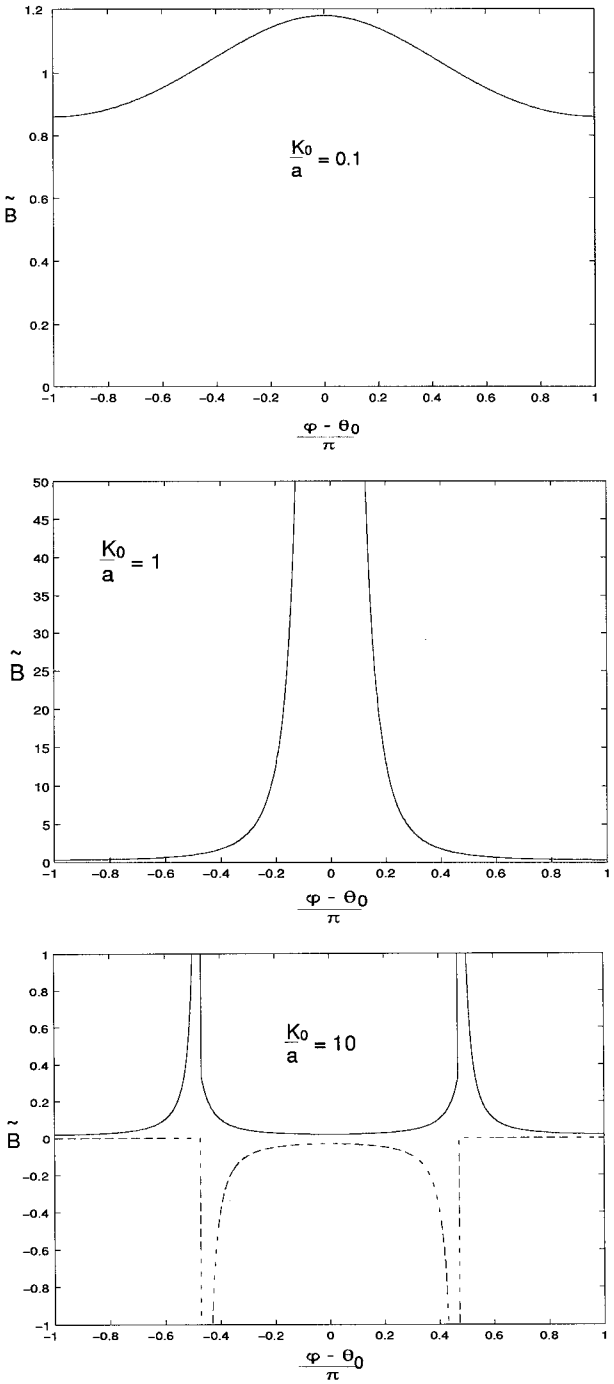

FIG. 4. As in Fig. 3 but for frequencies smaller than the maximal Rossby wave frequency.

$$C_{pF}(\Delta x, \Delta y, \omega) = \int dx' \int dy' G^*(x - x', y - y', \omega) \times C_{FF}(x + \Delta x - x', y + \Delta y - y', \omega). \quad (5.5)$$

Now the situation is different. The response at a point is due to forcing at many different locations, and the coherence squared

$$\gamma^2_{pF}(\Delta x, \Delta y, \omega) = \frac{|C_{pF}(\Delta x, \Delta y, \omega)|^2}{V_{pp}(\omega)V_{FF}(\omega)} \quad (5.6)$$

can be less than one, as a consequence of the Cauchy–Schwarz inequality. The reason for this is not that the relation between $p(x, y, \omega)$ and $F(x + \Delta x, y + \Delta y, \omega)$ is contaminated by noise or nonlinearities. The coherence between the response at (x, y) and the forcing at $(x + \Delta x, y + \Delta y)$ is degraded by forcing at other locations (x', y'). In (5.6), $V..(\omega)$ denotes the variance $C..(\Delta x = 0, \Delta y = 0, \omega)$.

The cross-spectrum $S_{pF}(k, l, \omega)$ is the Fourier transform of the cross-covariance function $C_{pF}(\Delta x, \Delta y, \omega)$. Both functions can thus be estimated from a single point ocean measurement and wind field maps. The reason that one uses $C_{pF}(\Delta x, \Delta y, \omega)$ and $\gamma^2_{pF}(\Delta x, \Delta y, \omega)$ rather than $S_{pF}(k, l, \omega)$ and $\gamma^2_{pF}(k, l, \omega)$ is that $V_{pp}(\omega)$ in the denominator of $\gamma^2_{pF}(\Delta x, \Delta y, \omega)$ can be estimated from single point ocean measurements, whereas $S_{pp}(k, l, \omega)$ in $\gamma^2_{pF}(k, l, \omega)$ cannot be estimated.

In quasigeostrophic theory the horizontal velocity components are given by $u = -\partial_y p$ and $v = \partial_x p$, except for a constant factor, and their Green's function by $G_u(k, l) = -ilG(k, l)$ and $G_v(k, l) = ikG(k, l)$. The cross-covariance functions between the velocity components and the forcing are therefore given by

$$C_{uF}(\Delta x, \Delta y) = \frac{\partial}{\partial \Delta y} C_{pF}(\Delta x, \Delta y) \quad (5.7a)$$

$$C_{vF}(\Delta x, \Delta y) = -\frac{\partial}{\partial \Delta x} C_{pF}(\Delta x, \Delta y, \omega) \quad (5.7b)$$

and are simply the meridional and zonal gradients of the cross-covariance function between pressure and forcing.

Brink (1989), Samelson (1990), and Lippert and Müller (1995) used formulas (5.5) and (5.6) and idealized wind covariance functions to calculate coherence maps. These calculated maps show decaying periodic structures with the principal maximum either at the mooring location or away from it, depending on the frequency and oceanic variable. Lippert and Müller (1995) asserted that the location of the maxima does not represent the location of the forcing, but that the maps represent interference patterns. Specifically, the different locations of the maxima in maps for *pF*, *uF*, and *vF* reflect the geostrophic relations (5.7) and not the fact that pressure and velocity signals are generated in different locations. In the resonance case, the maxima are located in the half plane such that the group velocity points toward the observer. In the next section we give simple examples to support these points.

6. Examples

If we express the cross-covariance function (5.5) in terms of the forcing spectrum

$$C_{pF}(\Delta x, \Delta y, \omega) = (2\pi)^2 \int dk \int dl G^*(k, l, \omega) \times S_{FF}(k, l, \omega) e^{i(k\Delta x + l\Delta y)}, \quad (6.1)$$

we see that cross-covariance maps represent the interference patterns of elementary "waves" $\exp[i(k\Delta x + l\Delta y)]$ with amplitude $G^*(k, l, \omega)S_{FF}(k, l, \omega)$. Coherence maps represent the normalized "intensity" pattern. These interference and intensity patterns reflect the scales of $G^*(k, l, \omega)$ and $S_{FF}(k, l, \omega)$. The parametric dependence on ω will again be dropped.

For forcing at a single wavenumber, $S_{FF}(k, l) = S_1\delta(k - k_1)\delta(l - l_1)$, we find

$$C^1_{pF}(\Delta x, \Delta y) = (2\pi)^2 G^*(k_1, l_1) e^{i(k_1\Delta x + l_1\Delta y)} S_1 \quad (6.2a)$$

$$V^1_{pp} = (2\pi)^4 G^*(k_1, l_1) G(k_1, l_1) S_1, \quad (6.2b)$$

and $V^1_{FF} = S_1$. Therefore $(\gamma^1_{pF}(\Delta x, \Delta y))^2 \equiv 1$. The coherences are identical to one for forcing at a single wavenumber.

For forcing at two wavenumbers, $S_{FF}(k, l) = S_1\delta(k - k_1)\delta(l - l_1) + S_2\delta(k - k_2)\delta(l - l_2)$, we find

$$C^{1+2}_{pF}(\Delta x, \Delta y) = (2\pi)^2 (G^*_1 S_1 e^{i(k_1\Delta x + l_1\Delta y)} + G^*_2 S_2 e^{i(k_2\Delta x + l_2\Delta y)}) \quad (6.3a)$$

$$V^{1+2}_{pp} = (2\pi)^4 (G^*_1 G_1 S_1 + G^*_2 G_2 S_2), \quad (6.3b)$$

and $V^{1+2}_{FF} = S_1 + S_2$ where $G_i = G(k_i, l_i)$. The coherence squared thus becomes

$$(\gamma^{1+2}_{pF}(\Delta x, \Delta y))^2 = \frac{G^*_1 G_1 S^2_1 + G^*_2 G_2 S^2_2 + S_1 S_2 (G^*_1 G_2 e^{i(k_1 - k_2)\Delta x} e^{i(l_1 - l_2)\Delta y} + \text{c.c.})}{(G^*_1 G_1 S_1 + G^*_2 G_2 S_2)(S_1 + S_2)} \quad (6.4)$$

and is generally less than one due to the interference of the two "waves." Consider specifically the case $S_1 = S_2$ and $k_2 = k_1$ and $l_2 = -l_1$, which implies $G_1 = G_2$. In this case

$$(\gamma^{1+2}_{pF}(\Delta x, \Delta y))^2 = \frac{1}{2}(1 + \cos(\Delta l \Delta y)) \tag{6.5}$$

with $\Delta l = l_2 - l_1$. The coherence squared is a periodic function of y with a maximum at the origin $\Delta y = 0$ and a periodicity given by the separation Δl of the forcing in wavenumber space. If (k, l) are chosen to be resonant wavenumbers, the response consists of two Rossby waves: one with a southward group velocity and all its signal coming from the north, and one with a northward group velocity and all its signal coming from the south. The location of the coherence maxima does not indicate the location of the forcing. This point becomes even more evident when we consider the coherence between the velocity components and the forcing. For our specific example, we find

$$\gamma^{1+2}_{uF}(\Delta x, \Delta y) = \gamma^{1+2}_{pF}(\Delta x, \Delta y) \tag{6.6a}$$

$$(\gamma^{1+2}_{uF}(\Delta x, \Delta y))^2 = \frac{1}{2}(1 - \cos(\Delta l \Delta y)). \tag{6.6b}$$

The coherence between p and F and between v and F has a maximum at the origin $\Delta y = 0$, whereas the coherence between u and F has a minimum at the origin, although the signals for u, v, and p all come from the same direction, as discussed in section 4.

The direction of the group velocity enters when we consider forcing in a small wavenumber band around a resonant wavenumber. Consider a coordinate system (k', l') such that the x axis coincides with the direction of the group velocity at (k'_0, l'_0). In this coordinate system, expansion of the resonance denominator about the resonant wavenumber (k'_0, l'_0) yields

$$\tilde{\omega}^* - \Omega(k', l') = \tilde{\omega}^* - \Omega(k'_0, l'_0) - V(k' - k'_0) + \cdots. \tag{6.7a}$$

$$\simeq -V\left(k' - k'_0 + \frac{i\nu}{V}\right), \tag{6.7b}$$

where $V = V(k'_0, l'_0)$ is the magnitude of the group velocity. The cross-covariance function then takes the form

$$C_{pF}(\Delta x', \Delta y') = -\frac{1}{V}\int dk' \int dl' \frac{1}{k' - k'_0 + \frac{i\nu}{V}} \frac{S_{FF}(k', l')}{k'^2 + l'^2 + R_o^{-2}} \times e^{i(k'\Delta x' + l'\Delta y')}. \tag{6.8}$$

In the limit $\nu \to 0$ we can substitute the integral representation

$$\lim_{\epsilon \to 0} \frac{1}{z + i\epsilon} = -i \int_0^\infty ds e^{isz} \tag{6.9}$$

for the resonance denominator. For a Gaussian forcing spectrum,

$$S_{FF}(k', l') = (k'^2 + l'^2 + R_o^{-2}) \frac{1}{2\pi \Delta k' \Delta l'} \times \exp\left\{-\frac{(k' - k'_0)^2}{2\Delta k'^2} - \frac{(l' - l'_0)^2}{2\Delta l'^2}\right\}, \tag{6.10}$$

the integration over l', k' and then over s can be carried out and results in

$$C_{pF}(\Delta x', \Delta y') = -\frac{1}{V} e^{i(k'_0 \Delta x' + l'_0 \Delta y')} \exp\left\{-\frac{1}{2}\Delta y'^2 \Delta l'^2\right\} \times \frac{\sqrt{\pi}}{2} \sqrt{2\Delta k'^{-2}}\, \mathrm{erfc}\left(\frac{\Delta x' \Delta k'}{\sqrt{2}}\right), \tag{6.11}$$

where $\mathrm{erfc}(x)$ is the complementary error function with $\mathrm{erfc}(-\infty) = 2$, $\mathrm{erfc}(0) = 1$, and $\mathrm{erfc}(\infty) = 0$. For $\Delta k' \to 0$ the cross-covariance function is unequal from zero only in the half-plane with the group velocity vector pointing toward the observer, consistent with the finding in section 4 about the origin of the signal.

A less trivial example is given by meridionally uniform forcing with spectrum

$$S_{FF}(k, l) = \frac{1}{k^2 + k_0^2}\delta(l) \tag{6.12}$$

or covariance function

$$C_{FF}(\Delta x, \Delta y) = \frac{\pi}{k_0} e^{-k_0|\Delta x|}. \tag{6.13}$$

The cross-covariance function then takes the form

$$C_{pF}(\Delta x, \Delta y) = -\frac{1}{\tilde{\omega}^*}\frac{1}{\tilde{a}^*_-}\frac{\pi}{k_0}\begin{cases}[(i\tilde{k}^*_a + k_0)^{-1} - (i\tilde{k}^*_b + k_0)^{-1}]e^{-k_0\Delta x} + [(i\tilde{k}^*_b + k_0)^{-1} - (i\tilde{k}^*_b - k_0)^{-1}]e^{i\tilde{k}^*_b\Delta x} & \text{for } \Delta x > 0 \\ [(i\tilde{k}^*_a - k_0)^{-1} - (i\tilde{k}^*_b - k_0)^{-1}]e^{k_0\Delta x} + [(i\tilde{k}^*_a + k_0)^{-1} - (i\tilde{k}^*_a - k_0)^{-1}]e^{i\tilde{k}^*_a\Delta x} & \text{for } \Delta x < 0. \end{cases} \tag{6.14}$$

For $|\omega| < \omega_{\max}$

$$\tilde{k}_{a,b} = k_{a,b} + i\frac{\nu}{V_{a,b}} \tag{6.15}$$

to lowest order in ν/ω, where

$$V_a = \frac{\omega a}{k_a k_c} > 0 \tag{6.16a}$$

$$V_b = -\frac{\omega a}{k_b k_c} < 0 \tag{6.16b}$$

are the group velocities at the resonant wavenumbers k_a and k_b. The cross-covariance map thus contains the decay scale k_0^{-1} arising from the bandwidth of the forcing spectrum and the periodicity scales $k_{a,b}^{-1}$ and frictional decay scales $V_{a,b}/\nu$ arising from the Green's function.

7. Multiple coherence

From an observational point of view, one only has the cross-covariance function $C_{pF}(\Delta x, \Delta y)$ and the autocovariance function $C_{FF}(\Delta x, \Delta y)$ of the wind forcing. If one postulates a linear relationship between the response at the mooring location and the forcing at other locations via a Green's function, as in (3.1), then one can perform a linear multiple regression analysis in order to estimate the Green's function. The best estimate $\tilde{G}(x, y)$ for the Green's function, in a least squares sense, is then given by

$$C_{pF}(\Delta x, \Delta y) = \int dx' \int dy' \tilde{G}^*(x - x', y - y') \times C_{FF}(x + \Delta x - x', y + \Delta y - y'), \tag{7.1}$$

which is identical to (5.5) except that the formula now contains $\tilde{G}$, which is to be estimated. The actual inversion or deconvolution of (7.1) in order to obtain $\tilde{G}(x, y)$ might be a complicated matter. However, (7.1) allows us to estimate how well the postulated linear relationship between forcing and response is supported by the observations. For this consider the difference

$$\epsilon = p(x, y) - \int dx' \int dy' \times \tilde{G}(x - x', y - y')F(x', y') \tag{7.2}$$

between the observed pressure signal $p(x, y)$ and its best estimate from the linear multiple regression analysis. The variance of this difference is given by

$$\begin{aligned}\langle \epsilon^* \epsilon \rangle &= \langle p^*(x, y)p(x, y)\rangle - \int dx' \int dy' \tilde{G}^*(x - x', y - y')\langle p(x, y)F^*(x', y')\rangle \\ &\quad - \int dx' \int dy' \tilde{G}(x - x', y - y')\langle p^*(x, y)F(x', y')\rangle \\ &\quad + \int dx' \int dy' \int dx'' \int dy'' \tilde{G}^*(x - x', y - y')\tilde{G}(x - x'', y - y'')\langle F^*(x', y')F(x'', y'')\rangle \qquad (7.3a) \\ &= V_{pp}(x, y) - \int dx' \int dy' \tilde{G}^*(x - x', y - y')C_{pF}^*(x' - x, y' - y), \qquad (7.3b)\end{aligned}$$

since the third and fourth terms in (7.3a) cancel because of (7.1). The variance of the difference can also be written

$$\langle \epsilon^* \epsilon \rangle = V_{pp}(1 - \gamma^2), \tag{7.4}$$

where

$$\gamma^2 = \frac{\int dx' \int dy' \tilde{G}^*(x - x', y - y')C_{pF}^*(x' - x, y' - y)}{V_{pp}} \tag{7.5}$$

is called multiple coherence by Bendat and Piersol (1971). The multiple coherence is a number and measures to what extent the postulated linear relationship between response and forcing is contaminated by noise, nonlinearities, or other forcing fields.

8. Summary and conclusions

We have analyzed the information contained in cross-covariance or coherence maps. These maps display the cross covariance or coherence between the oceanic response at a single observation point and the forcing field at other points. We specifically considered the barotropic quasigeostrophic response to wind forcing calculated from a simple model, although the results can obviously be generalized to other systems. Coherence maps must be used when ocean measurements are only available at a single (or a few) mooring locations. Then one cannot

correlate the complete response field with the complete forcing field. Our major results are the following.

- The coherence maps show values less than one. This is not an indication that the relation between forcing and response is contaminated by noise or nonlinearities, which is not true for our simple model, but simply a consequence of forcing at other locations.
- The coherence maps show patterns with local maxima at the mooring location or nonlocal maxima away from it. For our statistically homogeneous forcing model these maxima do not indicate the location of the forcing but the maps represent interference patterns, which in turn reflect the scales of the forcing spectrum and of the Green's function. If we had assumed a bounded ocean, another scale would enter the problem, namely the width of the ocean basin.
- The primary information contained in the cross-covariance maps is the Green's function. The Green's function can be estimated from observed cross-covariance maps and the observed wind field by multiple regression analysis. So far, oceanographers have tested physically motivated Green's functions by calculating cross-covariance maps with them and comparing these calculated maps to observed maps.
- The presence of noise or nonlinearities in the relation between response and forcing can be inferred from the multiple coherence, which is a single number.

Acknowledgments. I would like to thank Ken Brink, Roger Samelson, and Angelika Lippert for stimulating and clarifying discussions on the subject. I would also like to thank Xianbing Liu for his help with the figures and manuscript. This work was supported by the Office of Naval Research.

REFERENCES

Bendat, J. S., and A. G. Piersol, 1971: *Random Data: Analysis and Measurement Procedures.* Wiley-Interscience, 407 pp.

Brink, K. H., 1989: Evidence for wind-driven current fluctuations in the western North Atlantic. *J. Geophys. Res.,* **94,** 2029–2044.

Chave, A. D., D. S. Luther, and J. H. Filloux, 1992: The barotropic electromagnetic and pressure experiment: I. Barotropic current response to atmospheric forcing. *J. Geophys. Res.,* **97,** 9565–9593.

Frankignoul, C., and P. Müller, 1979: Quasi-geostrophic response of an infinite beta-plane ocean to stochastic forcing by the atmosphere. *J. Phys. Oceanogr.,* **9,** 105–127.

Lippert, A., and P. Müller, 1995: Direct atmospheric forcing of geostrophic eddies. Part II: Coherence maps. *J. Phys. Oceanogr.,* **25,** 106–121.

Luther, D. S., A. D. Chave, J. H. Filloux, and P. F. Spain, 1990: Evidence for local and nonlocal barotropic responses to atmospheric forcing during BEMPEX. *Geophys. Res. Lett.,* **17,** 949–952.

Morse, P. M., and H. Feshbach, 1953. *Methods of Theoretical Physics.* McGraw-Hill, 1978 pp.

Müller, P., 1996: Stochastic forcing of quasi-geostrophic eddies. *Stochastic Modelling in Physical Oceanography,* R. Adler, P. Müller, and B. Rozovskii, Eds., Birkhäuser, 381–395.

Samelson, R. M., 1989: Stochastically forced current fluctuations in vertical shear and over topography. *J. Geophys. Res.,* **94,** 8207–8215.

——, 1990: Evidence for wind-driven current fluctuations in the eastern North Atlantic. *J. Geophys. Res.,* **95,** 11 359–11 368.

——, and B. Shrayer, 1991: Currents forced by stochastic winds with meridionally varying amplitude. *J. Geophys. Res.,* **96,** 18 425–18 429.

Willebrand, J., S. G. H. Philander, and R. C. Pacanowski, 1980: The oceanic response to large-scale atmospheric disturbances. *J. Phys. Oceanogr.,* **10,** 411–429.